

Localization and Membrane Topology of Coronavirus Nonstructural Protein 4: Involvement of the Early Secretory Pathway in Replication[∇]

M. Oostra, E. G. te Lintelo, M. Deijns, M. H. Verheije, P. J. M. Rottier, and C. A. M. de Haan*

Virology Division, Department of Infectious Diseases and Immunology, Utrecht University, Yalelaan 1, 3584 CL Utrecht, The Netherlands

Received 10 July 2007/Accepted 4 September 2007

The coronavirus nonstructural proteins (nsp's) derived from the replicase polyproteins collectively constitute the viral replication complexes, which are anchored to double-membrane vesicles. Little is known about the biogenesis of these complexes, the membrane anchoring of which is probably mediated by nsp3, nsp4, and nsp6, as they contain several putative transmembrane domains. As a first step to getting more insight into the formation of the coronavirus replication complex, the membrane topology, processing, and subcellular localization of nsp4 of the mouse hepatitis virus (MHV) and severe acute respiratory syndrome-associated coronavirus (SARS-CoV) were elucidated in this study. Both nsp4 proteins became N glycosylated, while their amino and carboxy termini were localized to the cytoplasm. These observations imply nsp4 to assemble in the membrane as a tetraspanning transmembrane protein with a Nendo/Cendo topology. The amino terminus of SARS-CoV nsp4, but not that of MHV nsp4, was shown to be (partially) processed by signal peptidase. nsp4 localized to the endoplasmic reticulum (ER) when expressed alone but was recruited to the replication complexes in infected cells. nsp4 present in these complexes did not colocalize with markers of the ER or Golgi apparatus, while the susceptibility of its sugars to endoglycosidase H indicated that the protein had also not traveled through the latter compartment. The important role of the early secretory pathway in formation of the replication complexes was also demonstrated by the inhibition of coronaviral replication when the ER export machinery was blocked by use of the kinase inhibitor H89 or by expression of a mutant, Sar1[H79G].

Positive-strand RNA viruses assemble their replication complexes in association with cellular membranes, which can be recruited from different host cell compartments. This membrane association is probably advantageous in providing a suitable microenvironment for viral RNA synthesis, in facilitating the recruitment of membrane-associated host proteins having roles in virus replication/transcription, or in interfering somehow with the activation of host defense mechanisms that can be triggered by double-stranded RNA (dsRNA) intermediates of RNA virus replication (60).

Coronaviruses are enveloped positive-strand RNA viruses that contain exceptionally large genomes, the largest among all known RNA viruses. The most notorious member of the coronavirus family is the severe acute respiratory syndrome-associated coronavirus (SARS-CoV), which caused a widespread outbreak of severe pulmonary infections and many deaths during 2003. The 5' two-thirds of the coronavirus genome is occupied by a very large gene specifying the replicase complex; the remaining one-third codes for structural and accessory ("group-specific") proteins, which are translated from a nested set of subgenomic mRNAs, a characteristic feature of coronaviruses. The subgenomic mRNAs contain identical 3' and 5' ends, the latter of which correspond to the 5' end of the genomic RNA and are produced via a process of discontinuous transcription (53).

The replicase gene is composed of two open reading frames (ORFs), ORF1a and ORF1b, which encode two precursor

polyproteins, pp1a and pp1ab. The latter is produced by a ribosomal frame shift at the end of ORF1a (10). The polyproteins are extensively processed by virus-encoded proteinases, giving rise to 16 mature nonstructural proteins (nsp's) (20, 73). The proteinase domains are located within the ORF1a-encoded nsp3 and nsp5 proteins. The papain-like proteinase (PLpro) encoded by nsp3 cleaves downstream of nsp1, nsp2, and nsp3, while the 3C-like main proteinase (Mpro) encoded by nsp5 is responsible for the release of all other nsp's (2, 18, 65). The nsp's encoded by ORF1b (nsp12 to nsp16) are directly involved in the replication and transcription of the genome. Several enzymatic functions of these nsp's have been characterized, like the RNA-dependent RNA polymerase (nsp12), RNA helicase (nsp13), exonuclease (nsp14), endoribonuclease (nsp15), and methyltransferase (nsp16) (4, 6, 13, 27–29, 40, 48, 56, 59, 74) (Fig. 1). Recently, a second RNA-dependent RNA polymerase activity was discovered residing in nsp8 (26). Furthermore, the crystallographic structures of SARS-CoV nps5, nsp7, nsp8, nps9, nsp10, and nsp15 have been determined (12, 30, 49, 63, 70, 72).

The nsp's assemble collectively into a membrane-bound replication complex, which is the site of de novo viral RNA synthesis (58, 68). Also, the virus-encoded structural nucleocapsid (N) protein (8, 67) and possibly several cellular proteins (57) are recruited to this complex, which accumulates at perinuclear regions and is associated with double-membrane vesicles (DMVs) (11, 21, 60). The origin of the DMVs has not unambiguously been established. Several cellular pathways and organelles, such as the endoplasmic reticulum (ER), Golgi complex, endosomal/lysosomal system, and autophagic pathway, have been implicated in the formation of the replication complexes (46, 58, 60, 67). In addition, despite the functional

* Corresponding author. Mailing address: Virology Division, Department of Infectious Diseases and Immunology, Utrecht University, Yalelaan 1, 3584 CL Utrecht, The Netherlands. Phone: 31 30 253 4195. Fax: 31 30 253 6723. E-mail: C.A.M.deHaan@vet.uu.nl.

[∇] Published ahead of print on 12 September 2007.

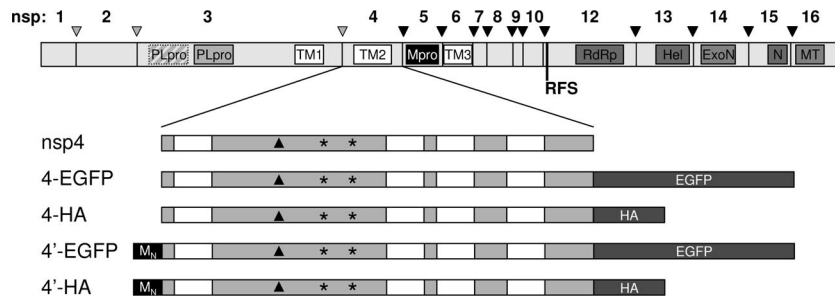


FIG. 1. Schematic representation of the coronavirus pp1ab polyprotein and of the nsp4 constructs used in this study. The coronavirus pp1ab precursor is shown at the top. The mature cleavage products (nsp's) are indicated by numbers. The transition between ORF1a and ORF1b is indicated as a ribosomal frame shift (RFS), while arrowheads represent sites that are cleaved by the nsp3-encoded PLpro protein (gray), of which there are two in MHV and only one in SARS-CoV, or by the nsp5-encoded Mpro protein (black). Within the nsp's, key replicate domains have been highlighted. These include putative transmembrane domains (TM) and the ORF1b-encoded domains: RNA-dependent RNA polymerase (RdRp), Helicase (Hel), exonuclease (ExoN), endoribonuclease (N), and methyltransferase (MT). The different nsp4 fusion proteins used in this study are schematically depicted below. nsp4 is shown in gray, with the hydrophobic domains in white, while asterisks indicate the approximate locations of the potential N glycosylation sites (NXS/T) in MHV nsp4 and the triangle indicates the approximate location of the atypical glycosylation motif (NXC) in SARS-CoV nsp4. The N (M_N)- and C (EGFP and HA)-terminal tags are also indicated.

characterization and structure determination of several nsp's, hardly anything is known about how the replication complexes are assembled and anchored to the DMVs.

The primary structures of three nsp's, nsp3, nsp4, and nsp6, contain hydrophobic stretches, and these proteins are predicted to be integral membrane proteins. Hence, they are likely to function in anchoring the replication complexes to the lipid bilayer. Indeed, for the nsp3 proteins of SARS-CoV (24) and mouse hepatitis virus (MHV) (32), membrane association has been demonstrated, while the modification of infectious bronchitis virus (IBV) nsp4 (37) by N-linked sugars is also indicative of membrane anchoring. However, detailed information on the membrane topology, processing, and subcellular localization of nsp4 is lacking. These features were elucidated in this study for MHV and SARS-CoV nsp4, resulting in more insight into the forming of the replication complex and its anchoring to the membrane.

MATERIALS AND METHODS

Cells, viruses, and antibodies. Murine LR7 cells (35), *Felis catus* whole fetus cells (American Type Culture Collection), and OST-7-1 cells (obtained from B. Moss) (17) were maintained as monolayer cultures in Dulbecco's modified Eagle's medium (DMEM) (Cambrex Bio Science Verviers, Belgium) containing 10% fetal calf serum (FCS) (Bodinco BV), 100 IU of penicillin, and 100 μ g of streptomycin per ml (referred to as culture medium). Recombinant vaccinia virus encoding the bacteriophage T7 RNA polymerase (vTF7-3) was obtained from B. Moss (19). The recombinant MHV carrying the feline infectious peritonitis virus spike ectodomain (fMHV) and the recombinant MHV with a firefly luciferase expression cassette (MHV-EFLM) have been described previously (16, 35).

Rabbit polyclonal antisera directed against the influenza virus hemagglutinin (HA) tag or enhanced green fluorescent protein (EGFP) were obtained from ICL. In addition, a rabbit polyclonal antiserum against EGFP was kindly provided by D. Duijsings and F. van Kuppeveld (Radboud University, Nijmegen, The Netherlands). The polyclonal antiserum against nsp8 (anti-p22) was kindly provided by M. Denison (39). The antibodies against calreticulin, GM130, and dsRNA were obtained from Sigma, Becton Dickinson, and English and Scientific Consulting Bt. (K1) (55), respectively. The rabbit antiserum recognizing the C-terminal domain of the MHV membrane (M) protein (αM_C) has been described previously (38), while the monoclonal antibody J1.3 against the amino terminus of MHV M (αM_N) was provided by J. Fleming (64).

Plasmid constructions. The SARS-CoV nsp4 gene fragment was obtained by reverse transcriptase PCR (RT-PCR) amplification of viral RNA isolated from SARS-CoV isolate 5688 (34), using primer 2982 (5'-CGATATCACCATGAAGATTGTTAGTACTGTGTTT, corresponding to nucleotides 8485 to 8505 of the

viral genome) and primer 2983 (5'-TTAGGATCCCTGCAGAACAGCAGAGT, corresponding to nucleotides 9984 to 9971). Both primers contain a 5' extension introducing either an EcoRV or a BamHI restriction enzyme recognition site (underlined), while additionally, a start codon is introduced in front of the nsp4-coding sequence (shown in bold). The PCR product was cloned into the pGEM-T Easy vector (Promega), resulting in construct pGem4_s, the sequence of which was confirmed by sequence analysis.

Subsequently, the nsp4 gene fragment was cloned in fusion with the EGFP gene into the pTUG31 (69) expression vector, which contains a bacteriophage T7 transcription-regulatory element. To this end, the nsp4 fragment was obtained by restriction with EcoRI and BamHI from pGem4_s, while the EGFP fragment was excised from the pEGFP-N3 vector (Clontech) by using BamHI and NotI, of which the latter restriction site was filled in with Klenow polymerase (Invitrogen). The two fragments were cloned into the EcoRI-SmaI-digested pTUG31 vector, creating pTug4_s-EGFP, which encodes SARS-CoV nsp4-EGFP.

In pTug4_s'-EGFP, an MHV M (M_N) tag-encoding sequence was inserted in front of the nsp4 gene by cloning a primer-dimer of primers 3019 (5'-TCGAGATTATGAGTAGTACTACGCAAGCCCCAGAGCCAGAT) and 3020 (5'-ATCTGGCTCTGGGGCTTGCCTAGTACTACTCATAATC), coding for the 10-residue amino-terminal sequence of the MHV M protein (MSSTTQAPEP) in the XhoI-EcoRV-restricted pTug4_s-EGFP vector, resulting in a construct which codes for SARS-CoV nsp4'-EGFP. The sequence encoding the EGFP tag in pTug4_s'-EGFP was replaced by an HA tag-encoding sequence by inserting a primer-dimer of primers 3050 (5'-GATCCTACCCATACGACGTGCCGACTATGCCTAG) and 3051 (5'-GATCCTAGGCATAGTCGGGCACGTCGTATGGGTAG) into the BamHI restriction sites flanking the EGFP-coding sequence, resulting in pTug4_s'-HA, which encodes SARS-CoV nsp4'-HA (see Fig. 1 for a schematic representation of the fusion proteins).

The putative N glycosylation site in SARS-CoV nsp4 (asparagine at amino acid position 131) was disrupted by site-directed mutagenesis (QuikChange II kit from Stratagene) using primers 3114 (5'-TTAGTCTGTTGGCGCCATTGCTACACAC) and 3115 (5'-GTGTGTAGCAAATGGCGCCAACAGCACTAA), with the mutations shown in bold, resulting in a construct that codes for SARS-CoV nsp4^{g131c}-EGFP.

The MHV nsp4 gene fragment was obtained by RT-PCR amplification of viral genomic RNA isolated from the MHV strain A59, using primer 2890 (5'-CCGATATCATGGCTGTTTTAGTAGAATGTTAC, corresponding to nucleotides 8721 to 8742 of the viral genome) and primer 2981 (5'-TTGGATCCCTGTAAAATGATGTAGTAACAGA, corresponding to nucleotides 10208 to 10183). Both primers contain a 5' extension introducing either an EcoRV or a BamHI restriction enzyme recognition site (underlined), while additionally, a start codon is introduced in front of the nsp4-coding sequence (shown in bold). The PCR product was digested with EcoRV and BamHI and ligated into the HindIII-BamHI-digested pEGFP-N3 vector (Clontech), the first restriction site of which was filled in with Klenow polymerase (Invitrogen), creating p4_m-EGFP-N3, which encodes MHV nsp4-EGFP. The nucleotide sequence of the PCR product was confirmed by sequence analysis.

The nsp4 gene fragment, in fusion with the EGFP gene, was cloned into the

pTUG31 expression vector, creating pTug_{4_m}-EGFP, also coding for MHV nsp4-EGFP. To this end, the nsp4-EGFP fragment was obtained from p_{4_m}-EGFP-N3 by digestion with XhoI and NotI, of which the latter restriction site was filled in with Klenow polymerase (Invitrogen), and cloned into the XhoI-SmaI-digested pTUG31 vector.

The M_N tag-encoding sequence was added to the 5' end of the MHV nsp4-EGFP fragment by excising the nsp4 and EGFP fragments from the pTug_{4_m}-EGFP construct with EcoRV and BamHI and cloning them into the EcoRV-BamHI-digested pTug_{4_s}-EGFP construct, thereby creating pTug_{4_m}'-EGFP, which encodes MHV nsp4'-EGFP. Subsequently, the sequence encoding the EGFP tag in this construct was replaced by the HA tag-encoding sequence by insertion of the primer-dimer of primers 3050 and 3051 in a way similar to that described above, resulting in construct pTug_{4_m}'-HA, which codes for MHV nsp4'-HA. p_{4_m}'-EGFP-N3, containing the N-terminally tagged MHV nsp4-EGFP fusion protein behind a cytomegalovirus promoter, was created by excising the 4_m'-EGFP fragment from pTug_{4_m}'-EGFP with XhoI and BamHI and cloning it into the XhoI-BamHI-digested pEGFP-N3 vector (Clontech).

The RNA transcription vector pMH54-nsp4-EGFP, which was used to create an MHV containing the gene encoding the MHV nsp4-EGFP fusion protein at the position of the HA esterase (HE) gene, was based on the previously described pMH54 vector (35). Two intermediate constructs were used to create this vector. First, an EGFP-encoding fragment obtained by digestion of the pEGFP-N3 vector (Clontech) with XbaI and NheI was cloned into the XbaI-NheI-digested pXH2509A plasmid, which has been described previously (16), resulting in pXH161202. The nsp4 gene fragment obtained from p_{4_m}-EGFP-N3 by digestion with NheI and BamHI was cloned into pXH161202 digested with the same enzymes. From the construct thus obtained, an AvrII-RsrII fragment was cloned into the AvrII-RsrII-digested pMH54 construct, resulting in pMH54-nsp4-EGFP. The transcription vector pERFPM, which was used for the generation of a recombinant MHV expressing a red fluorescent protein (RFP), was constructed essentially as described previously for pXHEFLM (16), with the exception that instead of the firefly luciferase gene, the gene encoding DsRed2 (Clontech) was used.

The construction of the vector encoding the equine arterivirus (EAV) membrane protein N-terminally extended with the M_N tag (EAV M+9A) has been described previously (15).

Generation of recombinant MHV. Incorporation of the nsp4-EGFP or the RFP expression cassette into the MHV genome by targeted RNA recombination was carried out as described previously (14, 25). Briefly, donor RNA transcribed from the linearized transcription vector was electroporated into *Felis catus* whole fetus cells that had been infected earlier with fMHV. These cells were plated onto a monolayer of murine LR7 cells. After 24 h of incubation at 37°C, progeny viruses released into the culture media were harvested and plaque purified twice on LR7 cells before a passage 1 stock was grown. After confirmation of the recombinant genotypes by RT-PCR on purified viral genomic RNA, a passage 2 stock that was subsequently used in the experiments was grown.

Infection and transfection. Subconfluent monolayers of LR-7 cells grown in 2-cm² tissue culture dishes were transfected by overlaying the cells with a mixture of 0.2 ml of DMEM without FCS but containing 1 μl of Lipofectamine 2000 (Invitrogen) and 1 μg of each selected construct, followed by incubation at 37°C. Three hours after transfection, the medium was replaced by culture medium. Where indicated, 24 h after transfection the cells were inoculated with MHV A59 or MHV-RFP at a multiplicity of infection (MOI) of 1 to 10 PFU per cell for 1 h, after which the inoculum was replaced by culture medium.

For expressions using the vTF7-3 system, subconfluent monolayers of OST7-1 cells grown in 10-cm² tissue culture dishes were inoculated with vTF7-3 at an MOI of 10 for 1 h, after which the medium was replaced by a transfection mixture consisting of 0.5 ml of DMEM without FCS but containing 10 μl of Lipofectin (Invitrogen) and 5 μg of each selected construct. After a 5-min incubation at room temperature, 0.5 ml of DMEM was added and incubation was continued at 37°C. Three hours after infection, the medium was replaced by culture medium and, where indicated, tunicamycin (5 μg/ml) or brefeldin A (6 μg/ml) was added to the medium.

For experiments with (recombinant) MHV, subconfluent monolayers of LR-7 cells grown in 2- or 10-cm² tissue culture dishes were inoculated with the recombinant virus at an MOI of 1 to 10 for 1 h, after which the inoculum was replaced by culture medium.

Metabolic labeling and immunoprecipitation. Prior to labeling, the cells were starved for 30 min in cysteine- and methionine-free modified Eagle's medium containing 10 mM HEPES (pH 7.2) and 5% dialyzed FCS. This medium was replaced by 1 ml of similar medium containing 100 μCi of ³⁵S in vitro cell-labeling mixture (Amersham), after which the cells were further incubated for the indicated time periods. After pulse labeling, the radioactivity was chased

from the cells where indicated, using culture medium containing 2 mM each of unlabeled methionine and cysteine. After pulse labeling or chase, the cells were washed once with phosphate-buffered saline (PBS) containing 50 mM Ca²⁺ and 50 mM Mg²⁺ and then lysed on ice in 1 ml of lysis buffer (0.5 mM Tris [pH 7.3], 1 mM EDTA, 0.1 M NaCl, 1% Triton X-100) per 10-cm² dish. The lysates were cleared by centrifugation for 5 min at 15,000 rpm and 4°C.

In vitro transcription and translation reactions were performed using the TNT coupled reticulocyte lysate system from Promega, according to the manufacturer's instructions, in the presence of a ³⁵S in vitro cell-labeling mixture (Amersham) but without the use of microsomal membranes.

Radioimmunoprecipitations were essentially performed as described previously (44); 200-μl aliquots of the cell lysates or 5 μl of in vitro translation reactions was diluted in 1 ml detergent buffer (50 mM Tris [pH 8.0], 62.5 mM EDTA, 1% NP-40, 0.4% sodium deoxycholate, 0.1% sodium dodecyl sulfate [SDS]) containing antibodies (3 μl rabbit anti-EGFP serum or rabbit anti-HA serum or 25 μl of the J1.3 monoclonal anti-MHV M serum). The immunoprecipitation mixtures were incubated overnight at 4°C. The immune complexes were adsorbed to Pansorbin cells (Calbiochem) for 60 min at 4°C and were subsequently collected by centrifugation. The pellets were washed three times by resuspension and centrifugation using radioimmunoprecipitation assay buffer (10 mM Tris [pH 7.4], 150 mM NaCl, 0.1% SDS, 1% NP-40, 1% sodium deoxycholate). The final pellets were suspended in Laemmli sample buffer (LSB) and heated at 95°C for 1 min before analysis by SDS-polyacrylamide gel electrophoresis (PAGE) using 10 to 15% polyacrylamide gels.

Where indicated, immunoprecipitates were treated with peptide-N-glycosidase F (PNGaseF) or endoglycosidase H (endoH) (both from New England Biolabs). To this end, the final immunoprecipitation pellets were suspended in PBS instead of LSB, 2 μl PNGaseF or endoH was added, and the samples were incubated at 37°C for 1 h. Before analysis by SDS-PAGE, a one-half volume of a three-times-concentrated solution of LSB was added to the samples, which were then heated at 95°C for 1 min.

Immunofluorescence microscopy. OST7-1 or LR7 cells grown on glass coverslips were fixed at the indicated times after infection or transfection with 3% paraformaldehyde for 1 h at room temperature. The fixed cells were washed with PBS and permeabilized using either 0.1% Triton X-100 for 10 min at room temperature or 0.5 μg/ml digitonin {diluted in 0.3 M sucrose, 25 mM MgCl₂⁺, 0.1 M KCl, 1 mM EDTA, 10 mM PIPES [piperazine-N,N'-bis(2-ethanesulfonic acid)] [pH 6.8]} for 5 min at 4°C. Next, the permeabilized cells were washed with PBS and incubated for 15 min in blocking buffer (PBS-10% normal goat serum), followed by a 45-min incubation with antibodies directed against nsp8, MHV M, EGFP, HA, dsRNA, calreticulin, or GM130. After four washes with PBS, the cells were incubated for 45 min with either Cy3-conjugated donkey anti-rabbit immunoglobulin G antibodies (Jackson Laboratories), fluorescein isothiocyanate-conjugated goat anti-rabbit immunoglobulin G antibodies (ICN), or Cy3-conjugated donkey anti-mouse immunoglobulin G antibodies (Jackson Laboratories). After four washes with PBS, the samples were mounted on glass slides in FluorSave (Calbiochem). The samples were examined with a confocal fluorescence microscope (Leica TCS SP2).

Fluorescence-activated cell sorting analysis of coronavirus replication. LR7 cells were transfected as described above, with plasmids encoding either Sar1 or Sar1[H79G] fused to yellow fluorescent protein (YFP), which were kindly provided by R. Pepperkok (62). At 24 h posttransfection, the cells were infected with a recombinant MHV expressing RFP. At 2 h postinfection, the HR2 fusion inhibitor (1 μM) (7) was added to the culture media to prevent cell-cell fusion. The cells were harvested at 16 h postinfection, fixed in 3% paraformaldehyde for 30 min, and after two washes with PBS, analyzed by flow cytometric analysis.

RESULTS

Bioinformatics analysis. The MHV and SARS-CoV nsp4 proteins are 496 and 500 amino acids long, respectively, and have calculated molecular masses of approximately 56 kDa. Both proteins are predicted to contain four transmembrane domains (<http://www.cbs.dtu.dk/services/TMHMM/>), with both termini being projected at the cytoplasmic side of the membrane. The first transmembrane domain might function as a cleavable signal sequence in both proteins, with cleavage predicted to occur after amino acid 29 for the MHV protein and after amino acid 32 for the SARS-CoV protein (<http://www.cbs.dtu.dk/services/SignalP/>). The three other predicted

transmembrane domains are located between residues 280 and 400, leaving a cytoplasmic C-terminal tail of approximately 100 amino acids. The predicted positions of the transmembrane domains are indicated in Fig. 1. MHV nsp4 contains two N glycosylation consensus sequences (NXS/T) at positions 176 and 237, both between the first and second transmembrane domains. Such sequences are not present in SARS-CoV nsp4 (<http://www.cbs.dtu.dk/services/NetNGlyc/>), although an atypical glycosylation motif (NXC) occurs at position 131, again between the first and second putative transmembrane domains (Fig. 1).

Localization of nsp4 in the presence or absence of infection.

In virus-infected cells, mature nsp4 is released from pp1a and pp1ab upon cleavage by viral proteinases. In this study, the membrane topology and posttranslational processing of MHV and SARS-CoV nsp4 were studied by expression of ORF1a gene fragments coding for nsp4 rather than by expression of the complete ORF1a gene. Thus, nsp4 was studied by itself rather than in the context of the pp1a or pp1ab precursor proteins. To justify this strategy, the subcellular localization of MHV nsp4 was studied by expression *in trans* in the context of an MHV infection. When the protein was correctly folded and inserted into membranes, it was expected to localize to the MHV replication sites (47), for which nsp8, a cytoplasmic protein lacking transmembrane domains, served as a marker (9). As a control, the localization of expressed EGFP was studied as well.

LR-7 cells transfected with plasmid pEGFP-N3, p4_m-EGFP-N3, or p4_m'-EGFP-N3, which carries the EGFP, the MHV nsp4-EGFP, or the N-terminally tagged MHV nsp4-EGFP gene, respectively, under the control of a cytomegalovirus promoter, were infected with MHV-A59 at 24 h posttransfection. At 6 h postinfection, the cells were fixed and processed for immunofluorescence microscopy. The expressed EGFP exhibited a diffuse fluorescence throughout the cytoplasm and the nucleus, both in infected (Fig. 2) and in noninfected (data not shown) cells, consistent with the known localization of GFP. In contrast, the nsp4-EGFP fusion proteins were restricted to a reticular pattern, reminiscent of the ER, in uninfected cells (Fig. 2) (note that neighboring cells, but not the nsp4-EGFP-expressing cell, were infected). The localizations of these fusion proteins in infected cells were clearly different. Here, the proteins localized not only to the reticular pattern but also to dots, which colocalized with the nsp8 marker for the replication sites (Fig. 2). These results indicate that nsp4 expressed *in trans* is correctly folded and inserted into membranes, as the protein is drawn to the replication complexes, likely through bona fide interactions with other viral proteins. It thus appears that individually expressed nsp4, containing amino- and/or carboxy-terminal tags, is properly assembled into membranes, providing a valid system for studying the membrane topology and processing of this protein.

Biogenesis of MHV and SARS-CoV nsp4. The co- and post-translational processing of MHV and SARS-CoV nsp4 were studied by *in vitro* translation and by using the recombinant vaccinia virus bacteriophage T7 RNA polymerase (vTF7-3) expression system. To investigate the N-linked glycosylation of MHV and SARS-CoV nsp4, the EGFP or HA fusion proteins were expressed in the presence or absence of tunicamycin, which is an inhibitor of N-linked glycosylation, and/or the N-

linked glycans were removed using PNGaseF. OST7-1 cells were infected with vTF7-3, transfected with plasmids containing the nsp4-EGFP or nsp4-HA gene, and labeled with ³⁵S-labeled amino acids for 1 h, starting at 5 h postinfection. Cells were lysed and processed for immunoprecipitation with a rabbit polyclonal antiserum directed to the EGFP or HA tag. In parallel, *in vitro* translations were performed using the TNT coupled reticulocyte lysate system from Promega in the absence of membranes to analyze the electrophoretic mobilities of the full-length nonprocessed proteins.

As shown in Fig. 3A, the *in vitro* translations resulted in a single band of about 60 kDa for both proteins. This is lower than the calculated molecular masses of both fusion proteins (84 kDa), which is, however, not exceptional for hydrophobic proteins and results from increased binding of SDS. Previously, the native nsp4 protein was also found to migrate faster than expected in SDS-polyacrylamide gels (21, 47). Expression of the SARS-CoV nsp4-EGFP fusion protein consistently resulted in the appearance of fuzzy bands in gels. Though this has been reported more often for proteins containing multiple transmembrane domains, the reason for it and why it is not seen for the MHV analogue are unknown.

vTF7-3-mediated expression of the MHV nsp4-EGFP fusion protein in the absence or presence of tunicamycin resulted in proteins migrating with electrophoretic mobilities that were slower than or the same as that of the *in vitro* translation product, respectively (Fig. 3A). This observation indicates that the nsp4-EGFP fusion protein is N glycosylated. These results were confirmed by removal of the N-linked sugars using PNGaseF (data not shown). Indeed, MHV nsp4 contains two potential N-glycan acceptor sites between the first and the second transmembrane domain. In addition, the results indicate that the first transmembrane domain, which probably functions as a signal sequence, is not cleaved by signal peptidases, contrary to the prediction.

Processing of SARS-CoV nsp4 appeared to be somewhat more complex. When the nsp4-EGFP fusion protein was expressed using the vTF7-3 system, three protein species were detected. The slowest-migrating one (no. 1 in Fig. 3A) disappeared in the presence of tunicamycin, indicating that this species contained N-linked sugars. The other two species, which were not affected by tunicamycin, migrated in the gel with mobilities equal to (no. 2 in Fig. 3A) or slightly faster than (no. 3 in Fig. 3A) that of the *in vitro* translation product. The faster-migrating species might result from signal peptide cleavage of nsp4, which is indeed predicted for this protein.

To confirm the results on the processing of SARS-CoV nsp4, the experiment was repeated with the HA-tagged protein (4_s-HA), the different protein species of which become better separated during SDS-PAGE. The addition of N-linked sugars to SARS-CoV nsp4 was further studied by treating the immunoprecipitates with PNGaseF (Fig. 3B). Upon expression of SARS-CoV nsp4-HA by use of the vTF7-3 expression system, four rather than three protein species were detected. The lower two species (no. 2 and 3) migrated in the gel with mobilities equal to (no. 2) or slightly lower than (no. 3) that of the *in vitro* translation product and probably differed in the presence of the signal peptide. These species were not glycosylated, as they were still detected after tunicamycin treatment of the cells (data not shown) or PNGaseF treatment of the samples

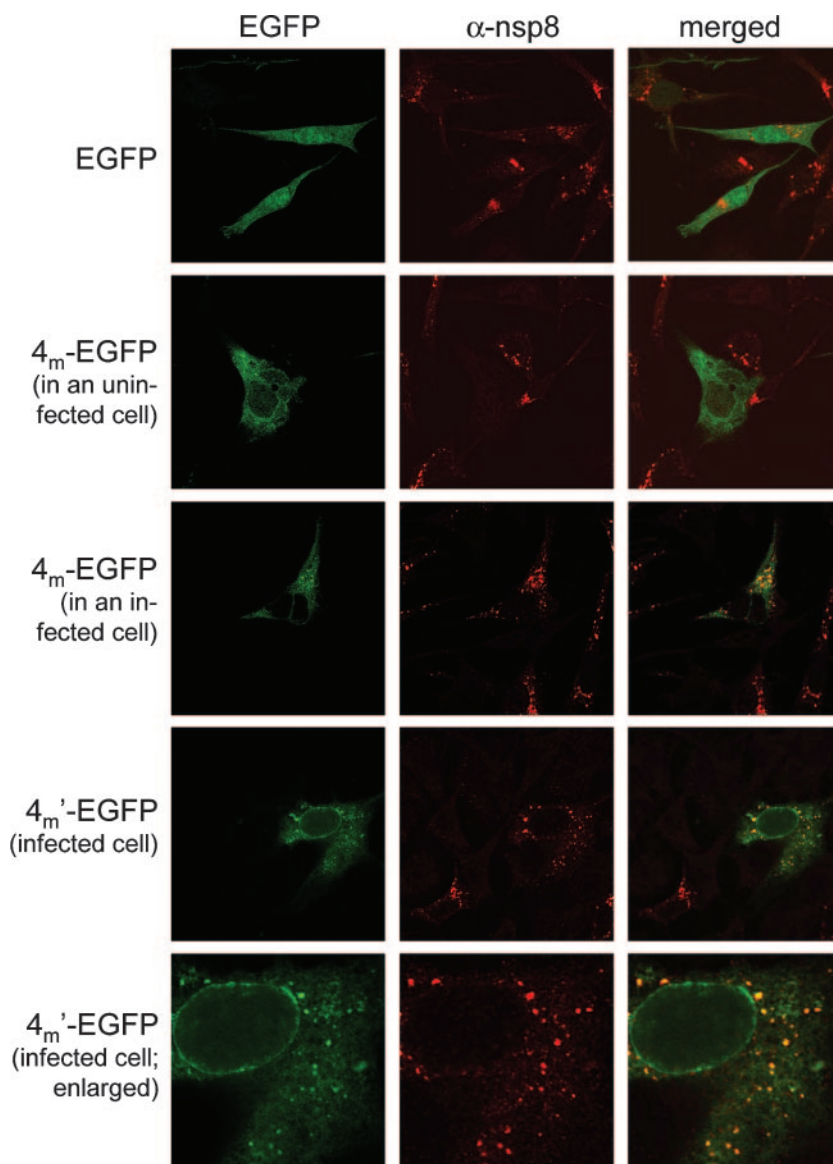


FIG. 2. Localization of transiently expressed nsp4. LR7 cells, transfected with EGFP-, MHV nsp4-EGFP (4_m -EGFP)-, or MHV nsp4'-EGFP ($4_m'$ -EGFP)-encoding constructs, were infected with MHV-A59. Cells were fixed at 6 h postinfection and processed for immunofluorescence microscopy using anti-nsp8 (α -nsp8) serum and a Cy3-conjugated antiserum to detect the MHV replication sites, as described in Materials and Methods. The second row shows a cell that is transfected (EGFP positive) but not infected (nsp8 negative), between cells that are infected (nsp8 positive) but not transfected (EGFP negative), whereas the lower rows show cells that are both transfected and infected (EGFP and nsp8 positive). At the right, a merged image of the α -nsp8 and the EGFP signal is shown. The bottom pictures are enlargements of the pictures in the row just above them.

(Fig. 3B), whereas the upper two protein species (no. 1a and 1b), which probably also differed in signal peptide cleavage, disappeared after treatment of the samples with tunicamycin (data not shown) or PNGaseF (Fig. 3B), confirming that these species contain N-linked sugars. Thus, SARS-CoV nsp4 is (incompletely) N glycosylated, even though this protein does not contain a classical N glycosylation consensus sequence (NXS/T). However, SARS-CoV nsp4 does contain an alternative glycosylation motif (NXC) between the first and second transmembrane domains. Upon replacement of the asparagine residue in this sequence by an alanine residue (nsp4^{-glyc}-HA), the slowest-migrating species were no longer detected (Fig. 3B),

confirming that this asparagine residue can indeed function as an N-glycan attachment site. The two glycosylated nsp4 species are likely to differ in their electrophoretic mobilities as a result of the incomplete cleavage of the signal peptide.

This putative (incomplete) signal peptide cleavage was studied further. To this end, a SARS-CoV nsp4 fusion protein containing an M_N tag consisting of the first 10 amino acids of the MHV M protein at its amino terminus and an HA tag at its carboxy terminus (nsp4'-HA) was expressed. Again, several protein species were detected after SDS-PAGE (Fig. 3B). While the upper two species (no. 1' and 2') migrated slightly slower than their nsp4 counterparts lacking the M_N tag, the

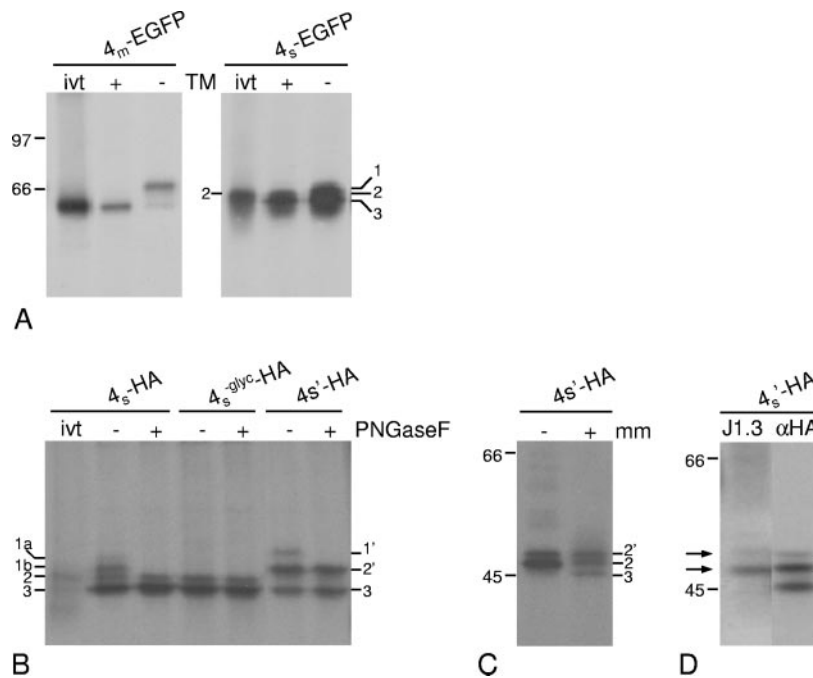


FIG. 3. Processing of MHV and SARS-CoV nsp4. vTF7-3-infected OST7-1 cells were transfected with the indicated constructs. The cells were labeled with ^{35}S -labeled amino acids from 5 to 6 h postinfection, lysed, and processed for immunoprecipitation with specific antibodies, followed by SDS-10% PAGE. (A) Cells were transfected with MHV or SARS-CoV nsp4-EGFP-encoding constructs (4_m -EGFP or 4_s -EGFP, respectively) in the presence (+) or absence (-) of tunicamycin (TM). The same constructs were also in vitro transcribed and translated using the TNT coupled reticulocyte lysate system from Promega (ivt). Immunoprecipitations were performed with rabbit antiserum against the EGFP tag. (B) Cells were transfected with constructs encoding SARS-CoV nsp4-HA (4_s -HA), a SARS-CoV nsp4-HA fusion protein containing a mutation of the NIC glycosylation motif (4_s -glyc-HA) or an N-terminally tagged SARS-CoV nsp4-HA fusion protein ($4_s'$ -HA). The construct encoding SARS-CoV nsp4-HA (4_s -HA) was also in vitro transcribed and translated using the TNT coupled reticulocyte lysate system from Promega (ivt). Immunoprecipitations were performed with rabbit serum against the HA tag, after which the samples were mock (-) or PNGaseF (+) treated. (C) The N-terminally tagged SARS-CoV nsp4-HA fusion protein was in vitro translated using the TNT coupled reticulocyte lysate system from Promega in the absence (-) or presence (+) of microsomal membranes (mm). (D) Cells were transfected with SARS-CoV nsp4 containing an N-terminal M_N tag and a C-terminal HA tag ($4_s'$ -HA). Immunoprecipitation with rabbit antiserum against the HA tag was followed, after boiling of the sample, by a second immunoprecipitation with either J1.3 antiserum against the N-terminal tag (J1.3; left lane) or the antiserum against the C-terminal HA tag (α -HA; right lane). The positions and masses (in kDa) of the molecular-mass protein markers are indicated, while the numbers 1, 2, and 3 indicate different SARS-CoV nsp4 species, of which the number 1 species are modified by N-linked sugars. The two arrows in panel D point to species 1' and 2', which are protein species containing the amino-terminal tag. Only the relevant portions of the gels are shown.

fastest-migrating form (no. 3) ran at exactly the same position in the gel as the fastest-migrating nsp4 protein without the amino-terminal tag. This is indeed expected when this protein species results from signal peptidase cleavage of the amino terminus. Next, this construct was expressed by in vitro translation in the absence or presence of membranes. In the absence of membranes, two protein species were detected (Fig. 3C), representing translation initiating either at the start codon of the N-terminal tag (no. 2') or at the next methionine residue directly in front of nsp4 (no. 2), as they ran slightly slower than or with the same mobility as the untagged, unprocessed nsp4-HA protein, respectively (data not shown). In the presence of membranes, however, an even faster-migrating protein species was detected, as expected when this protein is processed by signal peptidases.

Antibodies directed against the amino-terminal M_N tag are expected not to precipitate the nsp4 fusion protein after removal of the signal peptide. To demonstrate this point, a sequential immunoprecipitation assay was performed. After immunoprecipitation of all three SARS-CoV nsp4 species by use of antibodies directed against the HA tag (Fig. 3D), the im-

muno-precipitates were dissolved in a buffer containing β -mercaptoethanol and SDS and heated for 1 min at 95°C. Subsequently, the samples were processed for a second round of immunoprecipitation, using the J1.3 antibody against the N-terminal tag. While the J1.3 antibody was able to precipitate the larger two nsp4 species, this was no longer the case for the fastest-migrating form, demonstrating that the M_N tag was no longer present on this protein species (Fig. 3D).

All together, the results demonstrate that both the MHV and the SARS-CoV nsp4 proteins become inserted into the ER membrane, which results in the addition of N-linked sugars to their luminal domains. While their first transmembrane domain functions as a signal sequence, only the amino terminus of SARS-CoV nsp4 is subject to (partial) signal peptidase cleavage.

Topology of MHV and SARS-CoV nsp4. The observed N glycosylation of both nsp4 proteins shows that the region between the first and second transmembrane domains is exposed on the luminal side of the ER membrane. To determine the topology of MHV and SARS-CoV nsp4 in more detail, nsp4 proteins that were N-terminally extended with the M_N tag were

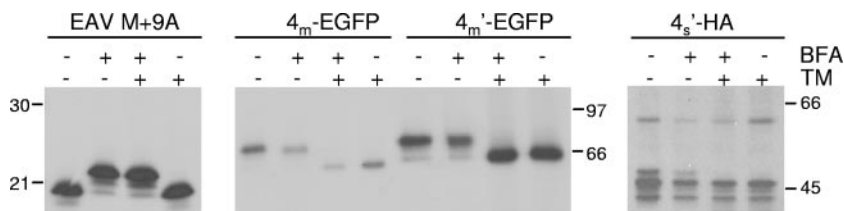


FIG. 4. O glycosylation of N-terminally tagged MHV and SARS-CoV nsp4. vTF7-3-infected OST7-1 cells were transfected with constructs encoding MHV nsp4-EGFP with or without the N-terminal tag ($4_m'$ -EGFP or 4_m -EGFP, respectively), N-terminally tagged SARS-CoV nsp4-HA ($4_s'$ -HA), or N-terminally tagged EAV M (EAV M+9A) in the presence (+) or absence (-) of tunicamycin (TM) and/or brefeldin A (BFA). The cells were labeled with ^{35}S -labeled amino acids from 5 to 6 h postinfection, and cell lysates were processed for immunoprecipitation with rabbit antiserum against EGFP or HA or, for EAV M, with J1.3, followed by SDS-10% PAGE. The positions of the molecular-mass protein markers are indicated on the left or right side of each gel. Only the relevant portions of the gels are shown.

used. This tag, which contains a well-defined O glycosylation site, has previously been appended onto the EAV type III M protein, resulting in EAV M+9A (15). Although this protein was retained in the ER, it became O glycosylated upon the addition of brefeldin A, a drug which causes redistribution of Golgi enzymes, including the ones involved in O glycosylation, to the ER.

By use of a similar approach, the location of the amino terminus of nsp4 was assessed. The EAV M+9A protein served as a positive control, while nsp4 proteins lacking N-terminal M_N tags were used as negative controls. The nsp4 fusion proteins were expressed using the vTF7-3 expression system with OST7-1 cells. Since the SARS-CoV nsp4-EGFP fusion protein appeared as rather fuzzy bands in the gel, the assay was also performed using the HA-tagged nsp4 protein. The proteins were labeled with ^{35}S -labeled amino acids from 5 to 6 h postinfection, after which the cells were lysed and processed for immunoprecipitation using polyclonal antisera directed to the EGFP or HA tag. The expressions were performed in the presence or absence of brefeldin A and/or tunicamycin. Tunicamycin was added to prevent N glycosylation, which could obscure the detection of O glycosylation. As expected, the electrophoretic mobility of nsp4 lacking the N-terminal tag was unaffected by the addition of brefeldin A (shown for MHV nsp4 only), while, as shown before, the presence of tunicamycin prevented the addition of N-linked sugars. In addition, nsp4 containing the M_N tag did not show an altered mobility upon the addition of brefeldin A ($4_m'$ -EGFP and $4_s'$ -HA), in contrast to the tagged EAV M (EAV M+9A) protein (Fig. 4).

These results indicate that the amino termini of MHV and SARS-CoV nsp4 are not accessible to enzymes that initiate the addition of O-linked sugars. While this is most likely to be caused by the lack of translocation of the amino-terminal end, one cannot rule out the possibility that the putative glycosylation sites are located too close to the membrane or that the amino terminus is folded such that the glycosylation sites are not accessible. We consider the latter options less likely, however, since the distances between the M_N tag and the predicted transmembrane domains in the nsp4 fusion proteins are similar to or even somewhat larger than those in the EAV M protein, while we have in addition previously demonstrated that the presence of the two proline residues in the tag induce a glycosylation-favorable conformation (15). Our interpretation of the amino terminus of nsp4 being exposed on the cytoplasmic

face of the ER is also in agreement with the observed N glycosylation of the region between the first and second transmembrane domains.

The localizations of the carboxy termini of both nsp4 proteins were determined by immunofluorescence assays in which antibodies directed against C-terminal tags (EGFP and HA) were used. To this end, OST7-1 cells were infected with vTF7-3, transfected with the nsp4-encoding plasmids, and fixed at 6 h postinfection using a 3% paraformaldehyde solution. Next, the cells were permeabilized using either Triton X-100, which permeabilizes all cellular membranes, or digitonin, which selectively permeabilizes the plasma membrane. The type III MHV M protein with its known topology (Nexo/Cendo) was used as a control. A rabbit polyclonal antibody directed to the C terminus (αM_C) and the J1.3 mouse monoclonal antibody directed to the N terminus of the MHV M protein were used to detect this protein after either Triton X-100 or digitonin permeabilization. As expected, the antibody directed to the C terminus detected the protein after Triton X-100 as well as after digitonin treatment, whereas the J1.3 antibody detected the protein only after permeabilization with Triton X-100, not after treatment with digitonin, thereby validating the assay conditions (Fig. 5).

When similar studies were done with the MHV and the SARS-CoV nsp4-EGFP fusion protein, in both cases all cells exhibiting GFP fluorescence stained positive with the antibody against the EGFP tag not only after permeabilization with Triton X-100 but also after treatment digitonin, indicating that the carboxy terminus of nsp4 is on the cytoplasmic face of the membrane (Fig. 5). This result was confirmed by using an HA-tagged nsp4 protein. In addition to the HA tag, this nsp4 protein also contained the M_N tag at its amino terminus. After permeabilization with either Triton X-100 or digitonin, the cells could be stained with the J1.3 monoclonal antibody and with the polyclonal HA antibody. The staining with the J1.3 antibody was weak but sufficient to detect the tagged MHV nsp4 protein. Clearly, both antibodies could detect the protein after permeabilization not only with Triton X-100 but also with digitonin (Fig. 5). In summary, the results demonstrate that both the amino and the carboxy termini of MHV and SARS-CoV nsp4 are exposed on the cytoplasmic face of the membrane.

Localization and processing of nsp4-EGFP expressed by recombinant MHV. To facilitate the study of the transport, localization, and processing of nsp4 in the context of a coro-

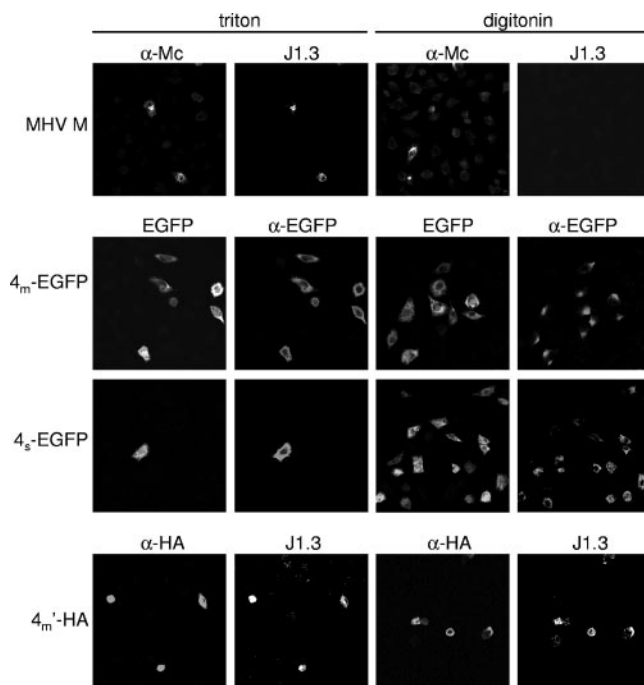


FIG. 5. Topology of MHV and SARS-CoV nsp4. vTF7-3-infected OST7-1 cells were transfected with constructs encoding the proteins indicated at the left. The cells were fixed at 6 h postinfection and permeabilized with Triton X-100 (left 2 columns) or digitonin (right 2 columns). Immunofluorescence analysis was performed with the antibodies indicated above the pictures, while EGFP indicates the EGFP fluorescence itself. α -Mc, anti-Mc; α -EGFP, anti-EGFP; α -HA, anti-HA.

navirus infection, a recombinant MHV in which the gene encoding the nsp4-EGFP fusion protein was incorporated into the viral genome using a targeted RNA recombination system previously described was constructed (14, 25). The nsp4-EGFP gene was placed at the position of the nonfunctional HE gene behind a transcription-regulatory sequence (Fig. 6A). The generated recombinant virus, which exhibited green fluorescent plaques, grew to titers similar to those of the wild-type virus, while the correct insertion of the nsp4-EGFP gene was confirmed by RT-PCR and sequence analysis.

The subcellular localization of the nsp4-EGFP fusion protein was studied in more detail using the newly generated recombinant virus. To this end, LR-7 cells were infected and fixed at the indicated time postinfection, after which the cells were processed for immunofluorescence microscopy. For all cells examined, the nsp4-EGFP fusion protein exhibited a reticular staining pattern and was additionally localized in dots (Fig. 6B and C), although some variability was observed in the intensity and number of dots between cells. nsp4-EGFP present in the dots colocalized with the nsp8 protein. To determine whether the nsp4-GFP/nsp8-positive dots also contained dsRNA intermediates produced during viral replication (53), cells were also labeled with monoclonal antibodies raised against dsRNA (55). Figure 6B shows that significant colocalization was observed between nsp4-EGFP present in the dots, nsp8, and dsRNA, demonstrating that nsp4-GFP localizes to the replication sites. As expected, the reticular staining of

nsp4-EGFP colocalized with the ER marker calreticulin (Fig. 6C), but this was not the case for the nsp4-EGFP protein present at the replication sites (Fig. 6C). Rather, the ER marker appeared to be excluded from these sites. Furthermore, nsp4-EGFP did not colocalize with the Golgi marker GM130. Essentially identical results were obtained when colocalization of nsp4-EGFP with the ER and Golgi markers was analyzed in HeLa cells (data not shown). The results show that the nsp4 protein, when expressed in *trans*, is localized to the ER and to the replication sites but not to the Golgi complex.

The intracellular fate of the nsp4 fusion protein was further investigated by analyzing the maturation of the N-linked sugars of the nsp4-EGFP protein (Fig. 7). LR7 cells were infected with the recombinant MHV expressing the nsp4-EGFP fusion protein and metabolically labeled for 1 h at 5 h postinfection, and where indicated, the radioactivity was chased for 90 min. Subsequently, the cells were lysed and processed for immunoprecipitation using the rabbit anti-EGFP serum. The precipitated proteins were treated with glycosidases to determine the maturation state of the N-linked glycans. While PNGaseF removes all N-linked carbohydrates, endoH is able to remove only N-linked glycans of the high-mannose type that have not been further modified by enzymes present in the medial or *trans*-Golgi compartment. Hence, resistance to endoH is indicative of transport of the protein through the medial and *trans*-Golgi cisternae. In Fig. 7, it is shown that the N-glycans attached to the nsp4 protein could be completely removed by both PNGaseF and endoH after the pulse as well as after the chase, demonstrating that the nsp4 protein did not travel through the medial and *trans* cisternae of the Golgi complex to reach its destination.

The role of the early secretory pathway in viral replication.

The above-described results indicate an important role for the early secretory pathway in the assembly of the coronavirus replication complexes. In order to corroborate this conclusion, the replication of MHV was analyzed in the presence of the kinase inhibitor H89. H89 is a specific inhibitor of protein kinase A at nanomolar concentrations, while it inhibits Sar1 recruitment to ER membranes in the micromolar range (3). Activation of the small GTPase Sar1 is required for export of proteins from the ER. MHV replication was monitored by analyzing the luciferase expression level after infection of cells with MHV-EFLM (16). The infected cells were treated with different concentrations of H89 from 1 to 6 h postinfection. At 6 h postinfection, the cells were lysed and the luciferase expression levels were determined. Clearly, treatment of cells with H89 at 50 μ M and higher concentrations resulted in a dramatic reduction of the luciferase expression level (Fig. 8A). The viability of the cells was not significantly affected by the H89 treatment, as determined by a WST-1 cell viability assay. We also studied whether coronavirus replication was affected early and/or late in the infection cycle. Cells infected with MHV-EFLM were treated with 50 μ M H89 from 1 to 4 or from 4 to 7 h postinfection. As is shown in Fig. 8B, coronavirus replication was severely inhibited by H89 during both time frames.

Next, the assembly of the coronavirus replication sites in the presence of H89 was analyzed using an immunofluorescence assay. To this end, LR7 cells were infected with MHV and at 4 h postinfection were either fixed or subjected to further

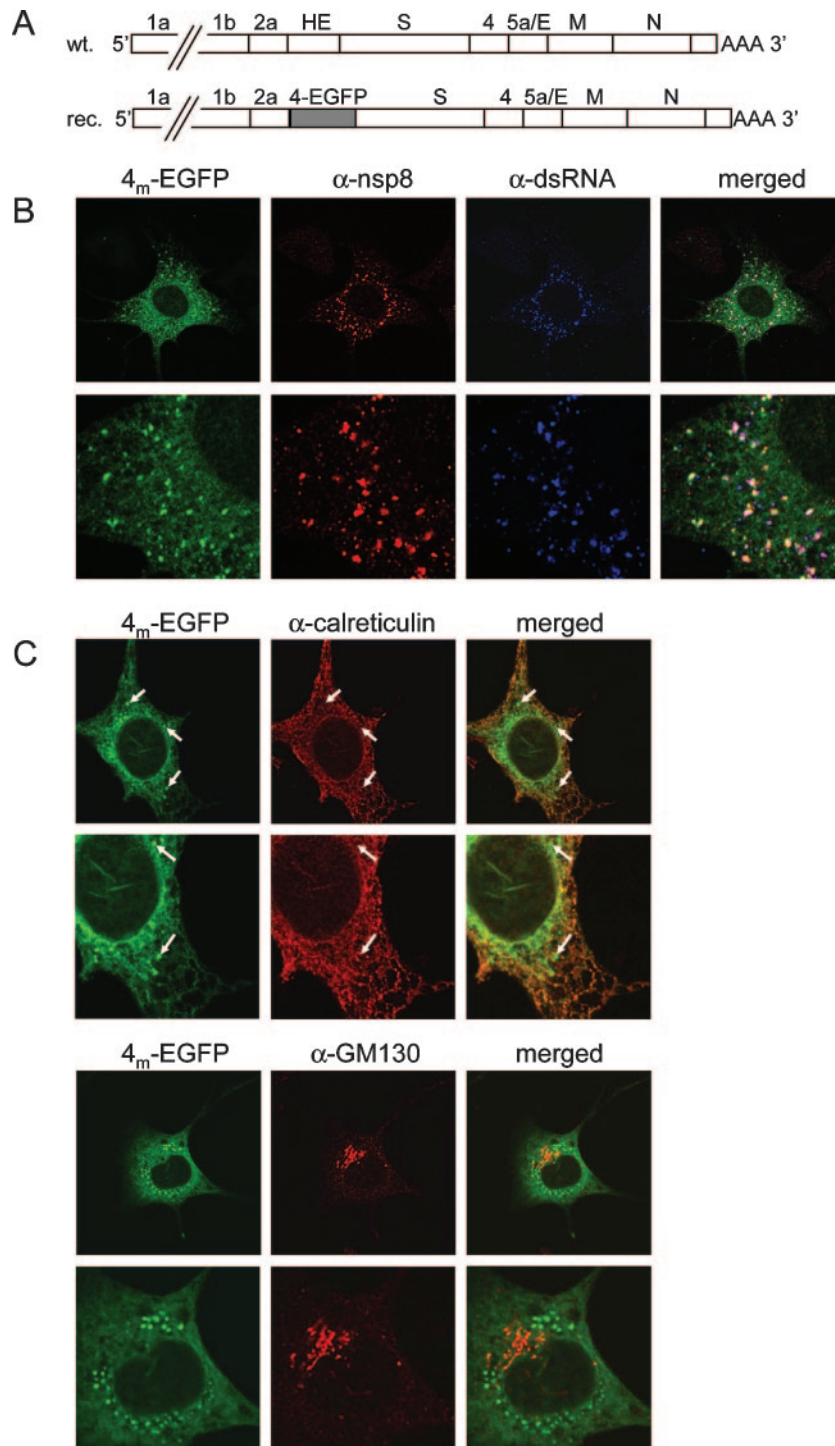


FIG. 6. Recombinant MHV containing nsp4-EGFP. (A) A recombinant MHV containing the MHV nsp4-EGFP fusion gene at the position of the HE gene was generated. The wild-type (wt) and recombinant (rec) MHV genomes are schematically represented. Genes are indicated by numbers or letters. AAA indicates the poly(A) tail at the 3' end. (B, C) LR7 cells were infected with the recombinant virus, fixed at 6 h (B) or 8 h (C) postinfection, and stained with antibodies against marker proteins: anti-nsp8 (α -nsp8), anti-dsRNA (α -dsRNA), anti-calreticulin (α -calreticulin) (ER), or anti-GM130 (α -GM130) (Golgi apparatus). Merged images of the EGFP signal with the staining of the different markers are shown at the right. In each set, the lower pictures are enlargements of the images above. The white arrows in the upper part of panel C indicate nsp4-EGFP located at the replication sites.

incubation at 37°C for 3 h in the absence or presence of H89. After fixation, the cells were processed for immunofluorescence analysis using antibodies directed against dsRNA or nsp8. As is shown in Fig. 8C, at 4 h postinfection only very little

dsRNA and nsp8 staining could be observed, while at 7 h postinfection, the amounts of dsRNA and nsp8 had increased considerably. However, in the presence of H89, this increase was not observed. As a control, cells were treated with the

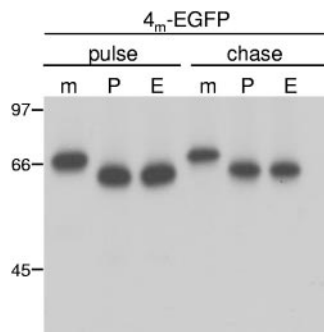


FIG. 7. Maturation of the glycosylation of nsp4. LR7 cells were infected with the recombinant MHV containing the nsp4-EGFP fusion gene (4_m -EGFP). The cells were labeled from 5 to 6 h postinfection (pulse), followed by a 90-min chase (chase), after which cell lysates were prepared and subjected to immunoprecipitation using the anti-EGFP antiserum. The immunoprecipitated material was treated with either PNGaseF (P) or EndoH (E) or was mock (m) treated. The numbers at the left indicate the positions of the molecular-mass protein markers. Only the relevant portion of the gel is shown.

protein synthesis inhibitor cycloheximide during the same time period. While, as expected, the amount of nsp8 did not change appreciably, a small increase in the dsRNA staining was observed. Indeed, as has been shown previously, at 4 h postinfection the addition of cycloheximide inhibits viral RNA synthesis, since the synthesis of both viral positive and minus strands requires continued protein synthesis (52). The results demonstrate that H89 inhibits coronavirus replication and the formation of replication sites.

To confirm the importance of Sar1, coronavirus replication was subsequently monitored in cells expressing a dominant mutant of Sar1 (Sar1[H79G]) in which ER exit is inhibited (1, 45). To this end, cells were transfected with plasmids expressing fusion proteins of YFP with either wild-type Sar1 or Sar1[H79G]. At 24 h posttransfection, the cells were infected with a recombinant MHV expressing RFP. When the RFP expression level was sufficiently high to allow efficient detection using fluorescence-activated cell sorting analysis, the percentage of transfected cells (YFP positive) that were productively infected (RFP positive) was determined. The results show that expression of the dominant mutant of Sar1 significantly inhibited coronavirus replication (Fig. 8D). Very similar results were obtained when the numbers of transfected and infected cells at 9 h postinfection were counted using fluorescence microscopy (data not shown). These data provide additional evidence for an important role for the early secretory pathway in coronavirus replication.

DISCUSSION

Coronaviruses replicate and transcribe their RNA by using intricate replication/transcription complexes which are made up of at least 16 nsp's and are associated with DMVs. The proteolytic processing of the polyprotein precursors of the nsp's has been extensively studied, and several enzymatic functions have been identified in the nsp's. However, relatively little is known about the formation of the replication complexes and their membrane association. Three nsp's (nsp3, nsp4, and nsp6) are predicted to contain transmembrane do-

main and are likely to be involved in membrane anchoring of the replication complex. Recently, the membrane association and topology of MHV nsp3 were reported (32). In this study, we focused on MHV and SARS-CoV nsp4, information on the membrane topology, processing, and subcellular localization of which was lacking until now.

The nsp4 sequence was cloned and expressed independently, i.e., not in the context of pp1a and pp1ab. This strategy allows the convenient addition of protein tags, without the need to worry about the proteolytic processing of pp1a and pp1ab, which could considerably complicate the interpretation of results. To verify the strategy, nsp4 was expressed in *trans* in the context of a viral infection. The protein was recruited to replication sites, probably via protein-protein interaction, indicating that it was correctly folded and inserted into membranes. Similar strategies have previously also been used to study the membrane topology of nsp's derived from large precursor polyproteins of other viruses, such as the dengue virus 4B protein (42). In addition, other coronavirus nsp's, lacking transmembrane domains, were also shown to be recruited to the replication sites when expressed in *trans* (11, 22).

While the processing of pp1a and pp1ab by the Mpro enzyme is relatively slow, cleavage by PLpro, which liberates the amino-terminal end of nsp4, is much faster. Indeed, in MHV-infected cells, proteolysis between nsp3 and nsp4 is the first cleavage event to be detected (21). Hence, the amino-terminal transmembrane domain of nsp4 is likely to function as a signal sequence. While for both the MHV and the SARS-CoV nsp4 protein a cleavable signal sequence is predicted, (partial) cleavage was observed only for the SARS-CoV nsp4. Cleavage of viral precursor polyproteins by signal peptidases is not uncommon, as it has been described, among others, for alphavirus membrane proteins (36) and for the generation of the amino termini of the flavivirus structural proteins prM and E as well as of their nsp1 and nsb4B proteins (42). The limited cleavage of SARS-CoV nsp4 by signal peptidase is, however, the first indication that coronavirus pp1a and pp1ab can be processed by proteins other than virus-encoded proteinases.

Upon integration into the ER membrane, the MHV and SARS-CoV nsp4 proteins become N glycosylated between the first and second transmembrane domains, implying that this domain is lumenally exposed (Fig. 9A). While two conventional consensus sequences (NXS/T) are present in MHV nsp4, glycosylation of SARS-CoV nsp4 was demonstrated to occur at an asparagine residue present in an atypical glycosylation motif (NXC). The addition of N-linked sugars to the unconventional glycosylation site NXC was first described in 1982 for the bovine protein C (61) and has since been demonstrated for a few more proteins, like human CD69 (66). The IBV nsp4 protein has also been shown to be modified by the addition of N-linked carbohydrates (37); however, the presence of N glycosylation sites (NXS/T or NXC) does not appear to be strictly conserved among the coronavirus nsp4 luminal domains. This is in agreement with the notion that tunicamycin does not affect viral RNA synthesis appreciably (50).

Consistent with the region between the first and second transmembrane domains being located on the luminal side of intracellular membranes, MHV and SARS-CoV nsp4 proteins were found to have a membrane topology in which both the N and C termini are facing the cytosol (Fig. 9A). This is in

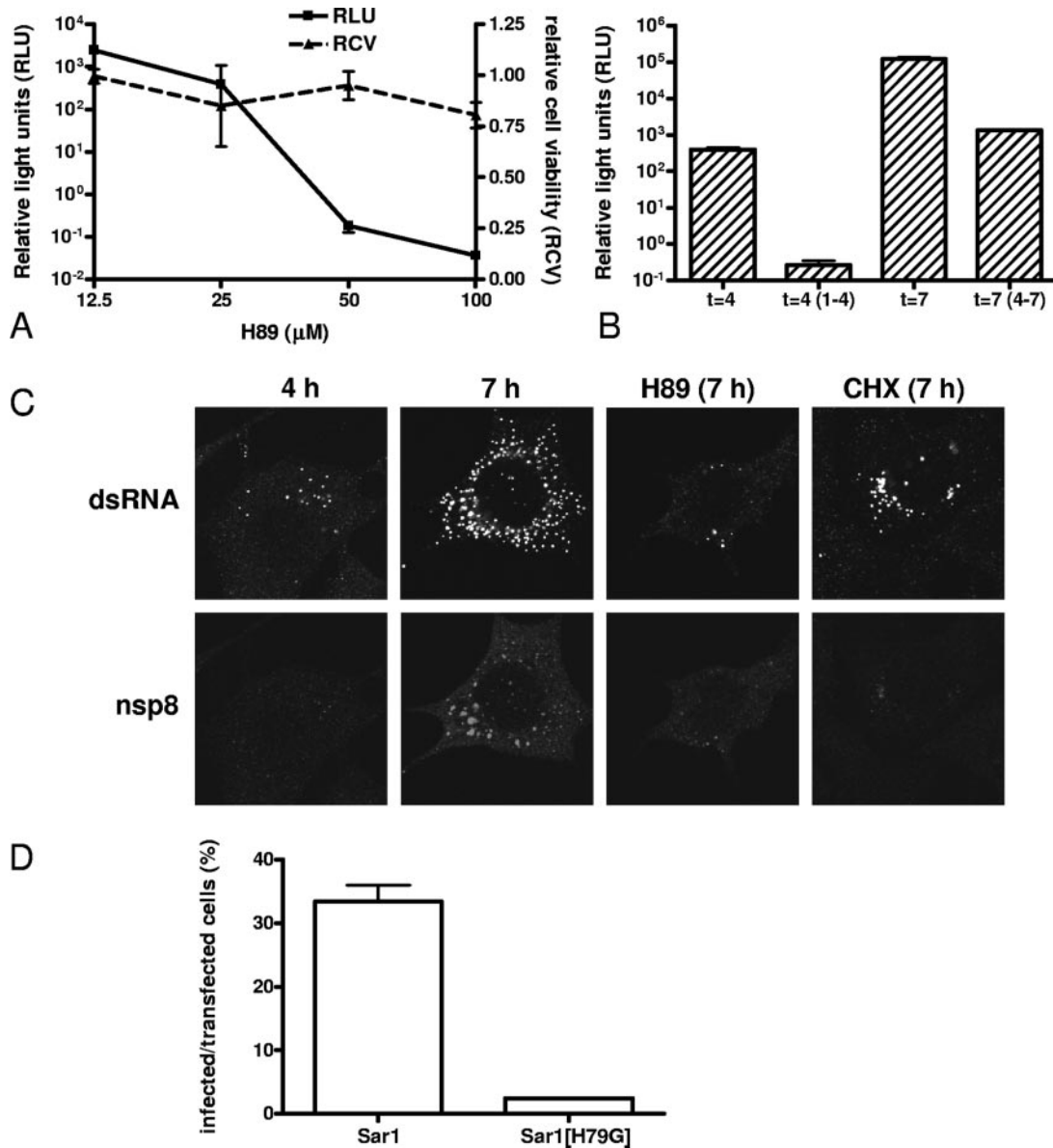


FIG. 8. Role of the early secretory pathway in virus replication. LR-7 cells were infected with MHV-EFLM in the presence of H89, and the viral replication was determined by measuring luciferase expression. (A) The cells were incubated with different concentrations of H89 from 1 to 6 h postinfection, after which luciferase activity was determined (left y axis). The cell viability was determined by a WST-1 assay (right y axis). (B) MHV-EFLM-infected cells were lysed at 4 (first two bars) or 7 (last two bars) h postinfection, either with (second and fourth bars) or without (first and third bars) 3 h of incubation with 50 μM H89. (C) At 4 h postinfection, LR-7 cells were infected with MHV and fixed (most left panels) or incubation at 37°C was continued for 3 h in the absence (7 h) or presence of H89 (H89) or cycloheximide (CHX). After fixation, the cells were processed for immunofluorescence analysis using antibodies directed against dsRNA or nsp8. (D) LR-7 cells were transfected with plasmids expressing fusion proteins of YFP with either wild-type Sar1 or Sar1[H79G] and 24 h later infected with a recombinant MHV expressing RFP. At 16 h postinfection, the number of RFP-positive cells in the YFP-positive population was determined by flow cytometric analysis.

agreement with nsp4 being a tetraspanning membrane protein. Although for some coronavirus nsp4 proteins one (IBV and human coronavirus NL63) or two (feline infectious peritonitis virus and human coronavirus 229E) additional transmembrane domains are predicted (<http://www.cbs.dtu.dk/services/TMHMM/>), four transmembrane domains are invariably predicted for the nsp4 protein equivalents of other nidoviruses, such as EAV, Berne torovirus, gill-associated okavirus, and white bream virus. It seems thus likely that, besides MHV and

SARS-CoV nsp4, the other coronavirus nsp4 proteins, as well as their nidovirus homologues, are tetraspanning transmembrane proteins with a Nendo/Cendo topology.

The topology of nsp4 implies that the enzymatic Mpro activity present in nsp5, which is located directly downstream of nsp4 in the polyprotein precursor, and which does not contain any transmembrane domains itself, remains localized to the cytoplasm. Since all Mpro cleavage sites should be accessible to the proteinase, all nsp's located downstream of the mem-

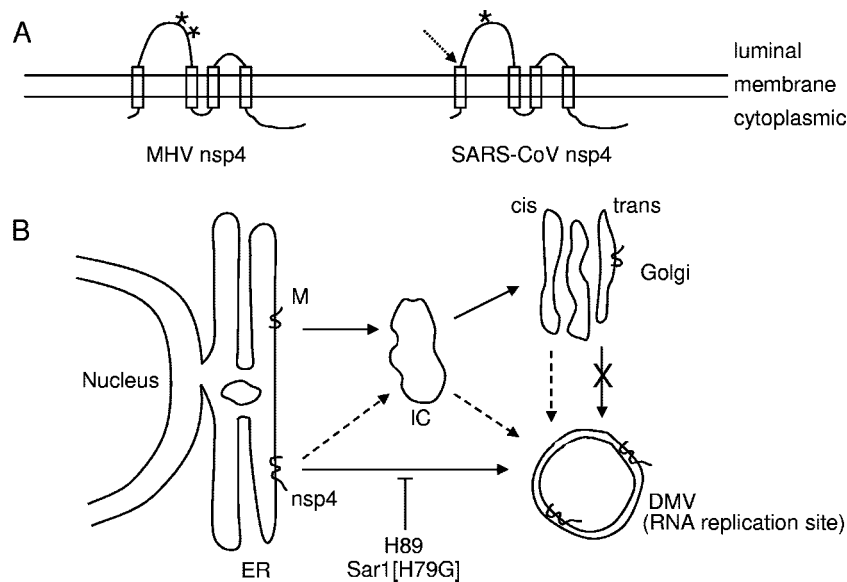


FIG. 9. Schematic representation of the proposed MHV and SARS-CoV nsp4 topology and intracellular transport. (A) The topology of MHV and SARS-CoV nsp4 is presented, with both the N and C termini at the cytoplasmic side of the membrane. The four predicted transmembrane domains are shown as white boxes, the N-glycosylation sites are presented as asterisks, and the (partial) signal sequence cleavage of the SARS-CoV nsp4 is indicated by the dotted arrow. (B) Intracellular localization and cellular transport are shown for nsp4 and for the coronavirus M protein. The M protein is transported from the ER to the Golgi compartment via the intermediate compartment (IC), whereas nsp4 is transported to the DMVs without passing through the medial or *trans* cisternae of the Golgi compartment. The inhibitory effect of H89 treatment or expression of Sar1[H79G] on coronavirus replication is indicated.

brane-anchored nsp6 protein, including the RNA-dependent RNA polymerase (nsp12) and RNA helicase (nsp13), which are directly involved in the replication of the viral RNA, must be in the cytoplasm as well. For the same reason, the amino-terminal half of nsp3, which contains the proteinase responsible for the proteolytic processing between nsp3 and nsp4, should also be located in the cytoplasm. Indeed, this is consistent with the proposed topology of MHV nsp3 (32). However, membrane topology predictions (<http://www.cbs.dtu.dk/services/TMHMM/>) of the complete coronavirus pp1a and pp1ab proteins depict a topology model in which the Mpro enzyme is separated from most of its cleavage sites by the lipid bilayer. Clearly, more experimental data are needed, particularly regarding the membrane topology of nsp6, for a better understanding of the polyprotein processing and generation of the replication complex.

Our results strongly suggest that the ER is the lipid donor compartment for the replication sites. The nsp4-EGFP fusion protein was localized to the ER when expressed alone but was additionally detected in the replication complexes, colocalizing with nsp8 and dsRNA, in the context of viral infection. Apparently, the fusion protein is recruited to the replication sites via interactions with other viral proteins. Strikingly, a previous study by Sawicki and coworkers (54) showed that a temperature-sensitive mutant of MHV nsp4 failed to be complemented by temperature-sensitive mutants in nsp5 or nsp10, which suggested either that the nsp4-to-nsp10 region functions as a polyprotein or that cleavage occurred in *cis* after association of the nsp4-to-nsp10 region to the replication sites. The nsp4-EGFP fusion protein localized in a reticular pattern as well as in dotted structures representing the replication sites. Overexpression of the nsp4-EGFP protein probably does not allow it

to be completely recruited to replication sites. The reticular nsp4-EGFP pattern colocalized with the ER marker calreticulin, while the fusion protein present in the replication sites did not colocalize with markers for the ER or Golgi complex (in both LR7 and HeLa cells), nor had it traveled through the Golgi complex. Consequently, the replication complexes either correspond with a specialized domain of the ER that lacks calreticulin or constitute a post-ER compartment, which is formed without the involvement of the medial and *trans* cisternae of the Golgi complex (Fig. 9B).

The importance of the early secretory pathway in the assembly of the replication sites was further confirmed by the inhibition of replication under conditions in which export from the ER was inhibited by the kinase inhibitor H89 or by overexpression of a mutant Sar1 protein. Sar1 is a small GTPase that plays an essential role in the formation of ER export domains and recruitment of COPII subunits (1, 23). The kinase inhibitor H89 inhibits the ER membrane association of Sar1 (3), thereby preventing export of cargo from the ER. Overexpression of the mutant Sar1[H79G], which is significantly reduced in its ability to hydrolyze GTP, also blocks productive ER-to-Golgi transport (62). While functional ER export machinery is clearly required for MHV replication, it remains to be determined whether Sar1 is directly or indirectly involved in the assembly of the replication complexes.

The involvement of the early secretory pathway in coronavirus replication is in agreement with previous reports which suggest that the DMVs with which the replication complexes are associated are derived from the ER compartment (58, 60). Other studies have implicated the involvement of the autophagic pathway in the formation of the replication complexes (46, 47). MHV-infected cells that lack a component of the autoph-

agy machinery (Atg5) and in which virus replication is severely impaired fail to induce DMVs. Rather, they exhibit dramatic effects on the structure of their ER, with hyperswollen membranes throughout the majority of the extremely altered cells (46). Coronaviruses might be able to exploit the protective mechanism of autophagy that is triggered by the accumulation of protein aggregates in the ER to generate the membrane structures that scaffold the replication complexes (31, 33, 71). However, while some studies demonstrated colocalization of the autophagy protein LC3/Atg8 with the replication sites (46, 47), this could not be confirmed by others (60).

All plus-strand RNA viruses replicate in association with intracellular membranes (5, 41, 43, 51). In many cases, the nsp's induce membrane invaginations or vesicles, which are thought to function as protective environments for RNA replication. The membranes not only provide an anchor for the replication complex but also appear essential for multiple steps during virus replication, as inhibitors of lipid synthesis also inhibit RNA replication by a number of viruses (5, 41, 43, 51), including coronaviruses (C. A. M. de Haan, unpublished results). However, until now only few mechanistic details explaining the transformation of the cellular membranes into the viral replication sites are understood. In the case of poliovirus, the dynamic association of several constituents of the early secretory pathway, including COPI and COPII components, has been implicated in the formation of the replication sites (5, 41, 43, 51). A similar role for the early secretory pathway in coronavirus replication seems plausible.

ACKNOWLEDGMENTS

We thank Matthijs Raaben and Marne Hagemeyer for stimulating discussions; D. Duijsings, F. van Kuppeveld, and M. Denison for providing antibodies; and R. Pepperkok for providing the Sar1 plasmids.

This work was supported by grants from The Netherlands Organization for Scientific Research (NWO-VIDI-700.54.421 to C. A. M. de Haan) and from the European Community (Frame VI, DISSECT PROJECT, SP22-CT-2004-511060 to P. J. M. Rottier).

REFERENCES

- Altan-Bonnet, N., R. Sougrat, and J. Lippincott-Schwartz. 2004. Molecular basis for Golgi maintenance and biogenesis. *Curr. Opin. Cell Biol.* **16**:364–372.
- Anand, K., J. Ziebuhr, P. Wadhvani, J. R. Mesters, and R. Hilgenfeld. 2003. Coronavirus main proteinase (3CLpro) structure: basis for design of anti-SARS drugs. *Science* **300**:1763–1767.
- Aridor, M., and W. E. Balch. 2000. Kinase signaling initiates coat complex II (COPII) recruitment and export from the mammalian endoplasmic reticulum. *J. Biol. Chem.* **275**:35673–35676.
- Baker, S. C., K. Yokomori, S. Dong, R. Carlisle, A. E. Gorbalenya, E. V. Koonin, and M. M. Lai. 1993. Identification of the catalytic sites of a papain-like cysteine proteinase of murine coronavirus. *J. Virol.* **67**:6056–6063.
- Belov, G. A., and E. Ehrenfeld. 2007. Involvement of cellular membrane traffic proteins in poliovirus replication. *Cell Cycle* **6**:36–38.
- Bhardwaj, K., L. Guarino, and C. C. Kao. 2004. The severe acute respiratory syndrome coronavirus Nsp15 protein is an endoribonuclease that prefers manganese as a cofactor. *J. Virol.* **78**:12218–12224.
- Bosch, B. J., R. van der Zee, C. A. de Haan, and P. J. Rottier. 2003. The coronavirus spike protein is a class I virus fusion protein: structural and functional characterization of the fusion core complex. *J. Virol.* **77**:8801–8811.
- Bost, A. G., R. H. Carnahan, X. T. Lu, and M. R. Denison. 2000. Four proteins processed from the replicase gene polyprotein of mouse hepatitis virus colocalize in the cell periphery and adjacent to sites of virion assembly. *J. Virol.* **74**:3379–3387.
- Bost, A. G., E. Prentice, and M. R. Denison. 2001. Mouse hepatitis virus replicase protein complexes are translocated to sites of M protein accumulation in the ERGIC at late times of infection. *Virology* **285**:21–29.
- Bredenbeek, P. J., C. J. Pachuk, A. F. Noten, J. Charite, W. Luytjes, S. R. Weiss, and W. J. Spaan. 1990. The primary structure and expression of the second open reading frame of the polymerase gene of the coronavirus MHV-A59; a highly conserved polymerase is expressed by an efficient ribosomal frameshifting mechanism. *Nucleic Acids Res.* **18**:1825–1832.
- Brockway, S. M., C. T. Clay, X. T. Lu, and M. R. Denison. 2003. Characterization of the expression, intracellular localization, and replication complex association of the putative mouse hepatitis virus RNA-dependent RNA polymerase. *J. Virol.* **77**:10515–10527.
- Campanacci, V., M. P. Eglöf, S. Longhi, F. Ferron, C. Rancurel, A. Salomoni, C. Dourousseau, F. Tocque, N. Bremond, J. C. Dobbe, E. J. Snijder, B. Canard, and C. Cambillau. 2003. Structural genomics of the SARS coronavirus: cloning, expression, crystallization and preliminary crystallographic study of the Nsp9 protein. *Acta Crystallogr. D* **59**:1628–1631.
- Cheng, A., W. Zhang, Y. Xie, W. Jiang, E. Arnold, S. G. Sarafianos, and J. Ding. 2005. Expression, purification, and characterization of SARS coronavirus RNA polymerase. *Virology* **335**:165–176.
- de Haan, C. A., P. S. Masters, X. Shen, S. Weiss, and P. J. Rottier. 2002. The group-specific murine coronavirus genes are not essential, but their deletion, by reverse genetics, is attenuating in the natural host. *Virology* **296**:177–189.
- de Haan, C. A., P. Roestenberg, M. de Wit, A. A. de Vries, T. Nilsson, H. Vennema, and P. J. Rottier. 1998. Structural requirements for O-glycosylation of the mouse hepatitis virus membrane protein. *J. Biol. Chem.* **273**:29905–29914.
- de Haan, C. A., L. van Genne, J. N. Stoop, H. Volders, and P. J. Rottier. 2003. Coronaviruses as vectors: position dependence of foreign gene expression. *J. Virol.* **77**:11312–11323.
- Elroy-Stein, O., and B. Moss. 1990. Cytoplasmic expression system based on constitutive synthesis of bacteriophage T7 RNA polymerase in mammalian cells. *Proc. Natl. Acad. Sci. USA* **87**:6743–6747.
- Fan, K., L. Ma, X. Han, H. Liang, P. Wei, Y. Liu, and L. Lai. 2005. The substrate specificity of SARS coronavirus 3C-like proteinase. *Biochem. Biophys. Res. Commun.* **329**:934–940.
- Fuerst, T. R., E. G. Niles, F. W. Studier, and B. Moss. 1986. Eukaryotic transient-expression system based on recombinant vaccinia virus that synthesizes bacteriophage T7 RNA polymerase. *Proc. Natl. Acad. Sci. USA* **83**:8122–8126.
- Gorbalenya, A. E., L. Enjuanes, J. Ziebuhr, and E. J. Snijder. 2006. Nidovirales: evolving the largest RNA virus genome. *Virus Res.* **117**:17–37.
- Gosert, R., A. Kanjanahaluthai, D. Egger, K. Bienz, and S. C. Baker. 2002. RNA replication of mouse hepatitis virus takes place at double-membrane vesicles. *J. Virol.* **76**:3697–3708.
- Graham, R. L., A. C. Sims, S. M. Brockway, R. S. Baric, and M. R. Denison. 2005. The nsp2 replicase proteins of murine hepatitis virus and severe acute respiratory syndrome coronavirus are dispensable for viral replication. *J. Virol.* **79**:13399–13411.
- Gurkan, C., S. M. Stagg, P. Lapointe, and W. E. Balch. 2006. The COPII cage: unifying principles of vesicle coat assembly. *Nat. Rev. Mol. Cell Biol.* **7**:727–738.
- Harcourt, B. H., D. Jukneliene, A. Kanjanahaluthai, J. Bechill, K. M. Severson, C. M. Smith, P. A. Rota, and S. C. Baker. 2004. Identification of severe acute respiratory syndrome coronavirus replicase products and characterization of papain-like protease activity. *J. Virol.* **78**:13600–13612.
- Hsue, B., and P. S. Masters. 1999. Insertion of a new transcriptional unit into the genome of mouse hepatitis virus. *J. Virol.* **73**:6128–6135.
- Imbert, I., J. C. Guillemot, J. M. Bourhis, C. Bussetta, B. Coutard, M. P. Eglöf, F. Ferron, A. E. Gorbalenya, and B. Canard. 2006. A second, non-canonical RNA-dependent RNA polymerase in SARS coronavirus. *EMBO J.* **25**:4933–4942.
- Ivanov, K. A., T. Hertzog, M. Rozanov, S. Bayer, V. Thiel, A. E. Gorbalenya, and J. Ziebuhr. 2004. Major genetic marker of nidoviruses encodes a replicative endoribonuclease. *Proc. Natl. Acad. Sci. USA* **101**:12694–12699.
- Ivanov, K. A., V. Thiel, J. C. Dobbe, Y. van der Meer, E. J. Snijder, and J. Ziebuhr. 2004. Multiple enzymatic activities associated with severe acute respiratory syndrome coronavirus helicase. *J. Virol.* **78**:5619–5632.
- Ivanov, K. A., and J. Ziebuhr. 2004. Human coronavirus 229E nonstructural protein 13: characterization of duplex-unwinding, nucleoside triphosphatase, and RNA 5'-triphosphatase activities. *J. Virol.* **78**:7833–7838.
- Joseph, J. S., K. S. Saikatendu, V. Subramanian, B. W. Neuman, A. Brooun, M. Griffith, K. Moy, M. K. Yadav, J. Velasquez, M. J. Buchmeier, R. C. Stevens, and P. Kuhn. 2006. Crystal structure of nonstructural protein 10 from the severe acute respiratory syndrome coronavirus reveals a novel fold with two zinc-binding motifs. *J. Virol.* **80**:7894–7901.
- Kamimoto, T., S. Shoji, T. Hidvegi, N. Mizushima, K. Umebayashi, D. H. Perlmuter, and T. Yoshimori. 2006. Intracellular inclusions containing mutant alpha-1-antitrypsin Z are propagated in the absence of autophagic activity. *J. Biol. Chem.* **281**:4467–4476.
- Kanjanahaluthai, A., Z. Chen, D. Jukneliene, and S. C. Baker. 2007. Membrane topology of murine coronavirus replicase nonstructural protein 3. *Virology* **361**:391–401.
- Kruse, K. B., J. L. Brodsky, and A. A. McCracken. 2006. Autophagy: an ER protein quality control process. *Autophagy* **2**:135–137.
- Kuiken, T., R. A. Fouchier, M. Schutten, G. F. Rimmelzwaan, G. van Amerongen, D. van Riel, J. D. Laman, T. de Jong, G. van Doornum, W. Lim,

- A. E. Ling, P. K. Chan, J. S. Tam, M. C. Zambon, R. Gopal, C. Drosten, S. van der Werf, N. Escriou, J. C. Manuguerra, K. Stohr, J. S. Peiris, and A. D. Osterhaus. 2003. Newly discovered coronavirus as the primary cause of severe acute respiratory syndrome. *Lancet* **362**:263–270.
35. Kuo, L., G. J. Godeke, M. J. Raamsman, P. S. Masters, and P. J. Rottier. 2000. Retargeting of coronavirus by substitution of the spike glycoprotein ectodomain: crossing the host cell species barrier. *J. Virol.* **74**:1393–1406.
 36. Liljeström, P., and H. Garoff. 1991. Internally located cleavable signal sequences direct the formation of Semliki Forest virus membrane proteins from a polyprotein precursor. *J. Virol.* **65**:147–154.
 37. Lim, K. P., L. F. Ng, and D. X. Liu. 2000. Identification of a novel cleavage activity of the first papain-like proteinase domain encoded by open reading frame 1a of the coronavirus Avian infectious bronchitis virus and characterization of the cleavage products. *J. Virol.* **74**:1674–1685.
 38. Locker, J. K., J. K. Rose, M. C. Horzinek, and P. J. Rottier. 1992. Membrane assembly of the triple-spanning coronavirus M protein. Individual transmembrane domains show preferred orientation. *J. Biol. Chem.* **267**:21911–21918.
 39. Lu, X. T., A. C. Sims, and M. R. Denison. 1998. Mouse hepatitis virus 3C-like protease cleaves a 22-kilodalton protein from the open reading frame 1a polyprotein in virus-infected cells and in vitro. *J. Virol.* **72**:2265–2271.
 40. Lu, Y., X. Lu, and M. R. Denison. 1995. Identification and characterization of a serine-like proteinase of the murine coronavirus MHV-A59. *J. Virol.* **69**:3554–3559.
 41. Mackenzie, J. 2005. Wrapping things up about virus RNA replication. *Traffic* **6**:967–977.
 42. Miller, S., S. Sparacio, and R. Bartenschlager. 2006. Subcellular localization and membrane topology of the Dengue virus type 2 non-structural protein 4B. *J. Biol. Chem.* **281**:8854–8863.
 43. Noueiry, A. O., and P. Ahlquist. 2003. Brome mosaic virus RNA replication: revealing the role of the host in RNA virus replication. *Annu. Rev. Phytopathol.* **41**:77–98.
 44. Oostra, M., C. A. de Haan, R. J. de Groot, and P. J. Rottier. 2006. Glycosylation of the severe acute respiratory syndrome coronavirus triple-spanning membrane proteins 3a and M. *J. Virol.* **80**:2326–2336.
 45. Pepperkok, R., M. Lowe, B. Burke, and T. E. Kreis. 1998. Three distinct steps in transport of vesicular stomatitis virus glycoprotein from the ER to the cell surface in vivo with differential sensitivities to GTP gamma S. *J. Cell Sci.* **111**:1877–1888.
 46. Prentice, E., W. G. Jerome, T. Yoshimori, N. Mizushima, and M. R. Denison. 2004. Coronavirus replication complex formation utilizes components of cellular autophagy. *J. Biol. Chem.* **279**:10136–10141.
 47. Prentice, E., J. McAuliffe, X. Lu, K. Subbarao, and M. R. Denison. 2004. Identification and characterization of severe acute respiratory syndrome coronavirus replicase proteins. *J. Virol.* **78**:9977–9986.
 48. Putics, A., W. Filipowicz, J. Hall, A. E. Gorbalenya, and J. Ziebuhr. 2005. ADP-ribose-1'-monophosphatase: a conserved coronavirus enzyme that is dispensable for viral replication in tissue culture. *J. Virol.* **79**:12721–12731.
 49. Ricagno, S., M. P. Egloff, R. Ulferts, B. Coutard, D. Nurizzo, V. Campanacci, C. Cambillau, J. Ziebuhr, and B. Canard. 2006. Crystal structure and mechanistic determinants of SARS coronavirus nonstructural protein 15 define an endoribonuclease family. *Proc. Natl. Acad. Sci. USA* **103**:11892–11897.
 50. Rottier, P. J., M. C. Horzinek, and B. A. van der Zeijst. 1981. Viral protein synthesis in mouse hepatitis virus strain A59-infected cells: effect of tunicamycin. *J. Virol.* **40**:350–357.
 51. Salonen, A., T. Ahola, and L. Kaariainen. 2005. Viral RNA replication in association with cellular membranes. *Curr. Top. Microbiol. Immunol.* **285**:139–173.
 52. Sawicki, S. G., and D. L. Sawicki. 1986. Coronavirus minus-strand RNA synthesis and effect of cycloheximide on coronavirus RNA synthesis. *J. Virol.* **57**:328–334.
 53. Sawicki, S. G., D. L. Sawicki, and S. G. Siddell. 2007. A contemporary view of coronavirus transcription. *J. Virol.* **81**:20–29.
 54. Sawicki, S. G., D. L. Sawicki, D. Younker, Y. Meyer, V. Thiel, H. Stokes, and S. G. Siddell. 2005. Functional and genetic analysis of coronavirus replicase-transcriptase proteins. *PLoS Pathog.* **1**:e39.
 55. Schonborn, J., J. Oberstrass, E. Breyel, J. Tittgen, J. Schumacher, and N. Lukacs. 1991. Monoclonal antibodies to double-stranded RNA as probes of RNA structure in crude nucleic acid extracts. *Nucleic Acids Res.* **19**:2993–3000.
 56. Seybert, A., C. C. Posthuma, L. C. van Dinten, E. J. Snijder, A. E. Gorbalenya, and J. Ziebuhr. 2005. A complex zinc finger controls the enzymatic activities of nidovirus helicases. *J. Virol.* **79**:696–704.
 57. Shi, S. T., and M. M. Lai. 2005. Viral and cellular proteins involved in coronavirus replication. *Curr. Top. Microbiol. Immunol.* **287**:95–131.
 58. Shi, S. T., J. J. Schiller, A. Kanjanahaluethai, S. C. Baker, J. W. Oh, and M. M. Lai. 1999. Colocalization and membrane association of murine hepatitis virus gene 1 products and de novo-synthesized viral RNA in infected cells. *J. Virol.* **73**:5957–5969.
 59. Snijder, E. J., P. J. Bredenbeek, J. C. Dobbe, V. Thiel, J. Ziebuhr, L. L. Poon, Y. Guan, M. Rozanov, W. J. Spaan, and A. E. Gorbalenya. 2003. Unique and conserved features of genome and proteome of SARS-coronavirus, an early split-off from the coronavirus group 2 lineage. *J. Mol. Biol.* **331**:991–1004.
 60. Snijder, E. J., Y. van der Meer, J. Zevenhoven-Dobbe, J. J. Onderwater, J. van der Meulen, H. K. Koerten, and A. M. Mommaas. 2006. Ultrastructure and origin of membrane vesicles associated with the severe acute respiratory syndrome coronavirus replication complex. *J. Virol.* **80**:5927–5940.
 61. Stenflo, J., and P. Fernlund. 1982. Amino acid sequence of the heavy chain of bovine protein C. *J. Biol. Chem.* **257**:12180–12190.
 62. Stephens, D. J., and R. Pepperkok. 2004. Differential effects of a GTP-restricted mutant of Sar1p on segregation of cargo during export from the endoplasmic reticulum. *J. Cell Sci.* **117**:3635–3644.
 63. Su, D., Z. Lou, F. Sun, Y. Zhai, H. Yang, R. Zhang, A. Joachimiak, X. C. Zhang, M. Bartlam, and Z. Rao. 2006. Dodecamer structure of severe acute respiratory syndrome coronavirus nonstructural protein nsp10. *J. Virol.* **80**:7902–7908.
 64. Taguchi, F., and J. O. Fleming. 1989. Comparison of six different murine coronavirus JHM variants by monoclonal antibodies against the E2 glycoprotein. *Virology* **169**:233–235.
 65. Thiel, V., K. A. Ivanov, A. Putics, T. Hertzog, B. Schelle, S. Bayer, B. Weissbrich, E. J. Snijder, H. Rabenau, H. W. Doerr, A. E. Gorbalenya, and J. Ziebuhr. 2003. Mechanisms and enzymes involved in SARS coronavirus genome expression. *J. Gen. Virol.* **84**:2305–2315.
 66. Vance, B. A., W. Wu, R. K. Ribaud, D. M. Segal, and K. P. Kearse. 1997. Multiple dimeric forms of human CD69 result from differential addition of N-glycans to typical (Asn-X-Ser/Thr) and atypical (Asn-X-cys) glycosylation motifs. *J. Biol. Chem.* **272**:23117–23122.
 67. van der Meer, Y., E. J. Snijder, J. C. Dobbe, S. Schleich, M. R. Denison, W. J. Spaan, and J. K. Locker. 1999. Localization of mouse hepatitis virus non-structural proteins and RNA synthesis indicates a role for late endosomes in viral replication. *J. Virol.* **73**:7641–7657.
 68. van der Meer, Y., H. van Tol, J. K. Locker, and E. J. Snijder. 1998. ORF1a-encoded replicase subunits are involved in the membrane association of the arterivirus replication complex. *J. Virol.* **72**:6689–6698.
 69. Vennema, H., R. Rijnbrand, L. Heijnen, M. C. Horzinek, and W. J. Spaan. 1991. Enhancement of the vaccinia virus/phage T7 RNA polymerase expression system using encephalomyocarditis virus 5'-untranslated region sequences. *Gene* **108**:201–209.
 70. Yang, H., M. Yang, Y. Ding, Y. Liu, Z. Lou, Z. Zhou, L. Sun, L. Mo, S. Ye, H. Pang, G. F. Gao, K. Anand, M. Bartlam, R. Hilgenfeld, and Z. Rao. 2003. The crystal structures of severe acute respiratory syndrome virus main protease and its complex with an inhibitor. *Proc. Natl. Acad. Sci. USA* **100**:13190–13195.
 71. Yorimitsu, T., U. Nair, Z. Yang, and D. J. Klionsky. 2006. Endoplasmic reticulum stress triggers autophagy. *J. Biol. Chem.* **281**:30299–30304.
 72. Zhai, Y., F. Sun, X. Li, H. Pang, X. Xu, M. Bartlam, and Z. Rao. 2005. Insights into SARS-CoV transcription and replication from the structure of the nsp7-nsp8 hexadecamer. *Nat. Struct. Mol. Biol.* **12**:980–986.
 73. Ziebuhr, J. 2005. The coronavirus replicase. *Curr. Top. Microbiol. Immunol.* **287**:57–94.
 74. Ziebuhr, J., E. J. Snijder, and A. E. Gorbalenya. 2000. Virus-encoded proteinases and proteolytic processing in the Nidovirales. *J. Gen. Virol.* **81**:853–879.